CHEMISTRY OF MATERIALS
Cite This: Chem. Mater. 2019, 31, 3900−3908
Article
pubs.acs.org/cm

Impact of Growth Conditions on the Phase Selectivity and Epitaxial Quality of TiO_2 Films Grown by the Plasma-Assisted Atomic Layer Deposition

Jason R. Avila,[†] Syed B. Qadri,[‡] Jaime A. Freitas, Jr.,[‡] Neeraj Nepal,[‡] David R. Boris,[‡] Scott G. Walton,[‡] Charles R. Eddy, Jr.,[‡] and Virginia D. Wheeler*[,‡]

[†]American Society for Engineering Education, 1818 N Street NW, Washington, District of Columbia 20018, United States
[‡]U.S. Naval Research Laboratory, Washington, District of Columbia 20375, United States

ABSTRACT: Plasma-enhanced atomic layer deposition (PE-ALD) is a promising method to grow conformal, epitaxial films at low temperatures (<300 °C). In this study, PE-ALD was used to deposit high-quality, epitaxial anatase and rutile TiO_2 thin films on sapphire substrates with various orientations (*c*-, *m*-, and *a*-Al_2O_3). For all substrate orientations, the influence of ALD growth temperature and plasma gas chemistry on the film morphology, phase, and crystallinity was investigated. On *c*-Al_2O_3, using a mixed Ar−O_2 plasma, the phase selectivity between anatase and rutile TiO_2 could be achieved by simply controlling the growth temperature from 150 to 350 °C. By using a pure O_2 plasma, single-phase rutile TiO_2 was grown independent of temperature or substrate orientation. Additionally, using a pure O_2 plasma resulted in higher crystalline quality films as growth temperatures were reduced, resulting in single-phase crystalline films at 150 °C. Although high-quality rutile films were attained on *c*- and *m*-Al_2O_3, only low-quality crystalline rutile films were produced on *a*-Al_2O_3. These results demonstrate the benefits of a PE-ALD approach toward depositing epitaxial TiO_2 under low-temperature conditions that is of high quality, phase and strain selective.

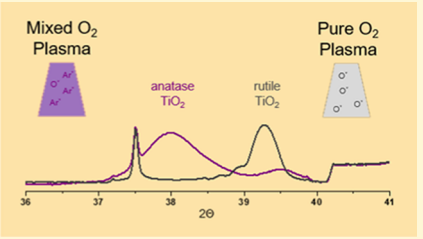

INTRODUCTION

TiO_2 is a well-studied material due in part to its high structural stability and tunable electronic properties.[1] The most common crystalline phases, anatase and rutile, present a promising low-cost material for a wide range of applications including catalysis,[2] semiconductor coatings,[3,4] photovoltaics,[5,6] and gate dielectrics.[7] Although there are a wide variety of techniques for depositing TiO_2, atomic layer deposition (ALD) has been shown to be a particularly useful method to achieve low-temperature, thin conformal films,[8] which has been deposited on a large variety of materials and architectures. Additionally, ALD is uniquely capable of adjusting simple growth conditions to achieve desired materials properties and crystalline quality, but often many deposition techniques require postdeposition annealing to achieve the desired crystallinity.

Although there are many reported methods for growing TiO_2 by ALD, there are significantly less on-growing crystalline TiO_2 and only a few based on depositing epitaxial TiO_2. Current reports on the conventional thermal ALD growth of epitaxial TiO_2 require either the use of halogenated Ti precursors[9,10] or elevated temperatures to achieve crystallinity,[8] both of which can be detrimental for certain applications. The drawback of halogenated precursors, such as $TiCl_4$, stems from the corrosive acidic byproduct when water is the co-reactant.[11−13] For example, the presence of HCl byproduct during the ALD growth with $TiCl_4$ can either incorporate Cl impurities or etch the underlying substrate, which can negatively impact the electronic properties for semiconductor applications. Growing TiO_2 at temperatures above 300 °C has been reported to reduce impurities for TiO_2 ALD processes using halogenated precursors[12,13] and facilitate the growth of crystalline TiO_2 using organometallic precursors, which produce less corrosive byproducts during ALD.[8,14] However, deposition at such elevated temperatures significantly limits the types of substrates with which TiO_2 can be integrated, such as InN, which is unstable at temperatures greater than 300 °C. Furthermore, many metals undergo migration and deleterious eutectics, and silicides can form at temperatures above 350 °C. Hence, there is still a need to develop a method for depositing epitaxial TiO_2 at lower deposition temperatures with less aggressive precursors.

Plasma-enhanced ALD (or PE-ALD) is a promising alternative process to enable the growth of crystalline TiO_2 at lower growth temperatures and allows for the use of organometallic Ti precursors. Currently, PE-ALD has been utilized to deposit the crystalline anatase TiO_2 using titanium tetraisopropoxide and tetrakis(dimethylamido)titanium (TDMAT).[15,16] However, to obtain the metastable rutile phase requires the use of specific substrates, such as Ru[17,18] or RuO_2,[18−20] or substrate biasing.[21,22] There is, however, a little reported research on the effects of the underlying substrate orientation on the phase and quality of the crystalline TiO_2 grown. Using PE-ALD, this study will demonstrate a controlled epitaxial

Received: December 21, 2018
Revised: May 13, 2019
Published: May 15, 2019

DOI: 10.1021/acs.chemmater.8b05282
Chem. Mater. 2019, 31, 3900−3908

growth of rutile and anatase crystalline phase TiO_2 and elucidate the effects of the underlying substrate orientation, growth temperature, and gas chemistry on the resulting film morphology, phase, and crystallinity.

EXPERIMENTAL SECTION

All ALD TiO_2 films were deposited on double-side polish, on-axis sapphire substrates (*c*-, *m*-, and *a*-plane oriented—MTI Corp) in a commercial Veeco Fiji G2 system using high-purity tetrakis-(dimethylamido)titanium (TDMAT, 99.99%-Ti, Strem Chemical) as a Ti source, an ultrahigh purity O_2 plasma as the co-reactant, and ultrahigh purity Ar as a carrier gas for the Ti source. All gases were purified further at the point of use. The TDMAT was heated to 75 °C and dosed for 25 ms with 10 s purge, whereas a 20 sccm O_2, 300 W plasma was dosed for 6 s with a 5 s purge. To investigate the impact of plasma gas chemistry, some films were deposited using the manufactured recommended gas conditions using a 4:1 Ar/O_2 gas flow ratio, which is labeled $Ar-O_2$ throughout the text. The rest of the films was deposited using a pure O_2 plasma, labeled O_2 throughout the text, and does not use Ar as a carrier gas during plasma operation. For all plasma gas compositions used, the total flow was kept at 20 sccm through the plasma source. Ar was always flowing through the plasma source during TDMAT dosing to ensure no precursor back flow. During TDMAT dosing, the Ar carrier gas was set to a flow rate of 30 sccm through the manifold and set to 10 sccm during plasma exposure. For both gas chemistries, ALD growths were conducted at growth temperatures (T_g) ranging from 150 to 350 °C. Additionally, for each deposition, ~43.2 ± 3.5 nm films were simultaneously grown on a set of *c*-, *m*-, and *a*-Al_2O_3 substrates along with a Si(100) witness substrate simultaneously.

To elucidate the impact of various parameters on the resulting materials properties of TiO_2 films, a variety of characterization methods were implemented. Film thickness was measured by spectroscopic ellipsometry on Si witness samples using a J. A. Woollam variable angle α spectrometer. Atomic force microscopy (AFM) was used to analyze the film morphology using a Dimension Fastscan (Bruker) in the tapping mode. Film phase, strain, and crystallinity were characterized using Raman spectroscopy and X-ray diffraction (XRD). Micro-Raman spectroscopy was conducted on a DXRxi Raman Imaging Microscope (Thermo Scientific) using a 532 nm laser with a power of 4 mW and a spot size of 0.7 um. XRD spectra were acquired on two different systems. Initial identification of film phase and orientation was accomplished with a low-resolution powder XRD (Rigaku) instrument with Cu Kα_1 radiation and a high-intensity point detector. 2θ spectra were collected by scanning from 15 to 90° with a step size of 0.02° at a scan speed of 0.04°/s. The high-resolution (HR) X-ray set up (Rigaku) consists of an 18 kW rotating anode and a four-circle diffractometer. The incident X-ray beam is a monochromatic Cu Kα_1 radiation obtained from two channel-cut Ge(220) crystals located on the incident beam optics. This arrangement provides the best resolution for accurate 2θ diffraction profiles. The diffraction profiles were collected by counting on each 2θ step of 0.1° for 50 s in a step-scan mode. For the asymmetric diffraction, the two high-order sapphire peaks, (0,2,10) and (2,1,10), were selected for the *c*-Al_2O_3 substrate, whereas only one sapphire peak, (2,2,6), was used for the *m*-Al_2O_3 substrate. The angles between (001) and (0,2,10) and (2,1,10) were 32.3 and 39.9°, with the angle of incidence for the X-ray beam and the substrate surface being 12.22 and 10.66°, respectively. The angle between (100) and (2,2,6) was calculated to be 40.6° with a corresponding angle of incidence of 7.06° between the substrate surface and the incident X-ray beam. The ω, ϕ, and ψ were optimized for the substrate peaks, and the X-ray profiles were obtained in $2\theta-\Psi$ where $\Psi = \theta - \psi$ and ψ is the angle between (001) and the sapphire peaks for the *c*-plane sapphire and the angle between (100) and the corresponding sapphire peaks for the *m*-plane sapphire. Grazing incidence diffractions (GID) were also measured using a Bruker three-circle platform diffractometer equipped with a PHOTON 100 CMOS detector. Substrates were suspended in Cargille NVH immersion oil, mounted on a MiteGen MicroMesh and irradiated using a 1 μs microfocus Cu Kα_1 source (λ = 1.54178 nm) with a Helios optics. Data was collected at room temperature (20 °C) to verify if there is any evidence of texturing or the presence of characteristic diffraction rings of a polycrystalline material.

Strain (ε) was calculated by the percentage difference (eq 1) of the *d* space (*d*) of the peak positions in XRD to the relaxed *d* spacing (d_r) of anatase [PDF 01-084-1285 (ICSD, 2017)][23] and rutile [PDF 01-078-1508 (ICSD, 2017)][24] TiO_2.

$$\varepsilon = \frac{d - d_r}{d_r} \times 100 \quad (1)$$

Using eq 1, a negative strain is indicative of a compressively strained film, whereas a positive strain indicates the film under the tensile strain. XPS spectra were obtained using a Thermo Scientific K-Alpha system. To counter any charging that could occur in these oxide films, a flood gun was implemented, and the C 1s peak was aligned to 289 eV. Both low-resolution survey and high-resolution core peak scans were measured. To confirm the impurities at the surface and within the film, samples were etched with a monotonic Ar ion gun at 1 keV with a low current for 30 s.

Finally, cathodoluminescence (CL) was used to study the defectivity of the deposited TiO_2 films. The CL set up consists of a commercial electron gun and a cold finger cryostat installed in an ultrahigh vacuum chamber with a vacuum typically $\leq 10^{-10}$ torr. The electron gun, fitted with a LaB_6 cathode to allow a small spot size (from 70 to 100 μm) and current up to 5 μA, can be operated on continuous-wave or pulsed mode with a beam energy between 0.1 and 20 keV. The sample temperature can be varied from 2 to 320 K. We used an accelerating voltage of 3 keV and current of 3 μA, to optimize the thin film excitation and reduce film heating. The light emitted by the sample under the electron beam excitation was dispersed by a single-grating fiber optics spectrometer, fitted with an extended UV sensitive charge-coupled device coupled to a computer for data acquisition and manipulation. The spectrometer calibration is verified with calibrated lines from an Hg lamp.

RESULTS AND DISCUSSION

The as-deposited TiO_2 film composition and impurity concentration were assessed by XPS (Figure 1 and Table 1).

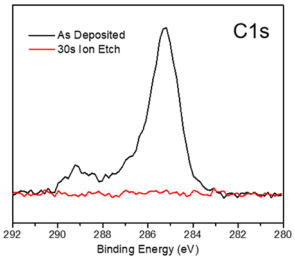

Figure 1. XPS C 1s spectra of TiO_2 as deposited (black) and after 30 s Ar ion etch (red).

Figure 1 shows the C 1s scan from typical TiO_2 films deposited, showing that after 30 s of ion etching, the carbon is below the detection limits of XPS. The surface carbon detected in the as-

Table 1. XPS Results for Films Grown with Both $Ar-O_2$ and O_2 Plasma Gas Chemistries

plasma gas	T_g (°C)	[Ti] (atom %)	[O] (atom %)	Ti/O_2
$Ar-O_2$	150	32.81	67.19	0.49
	250	32.84	67.16	0.49
	350	32.98	67.02	0.49
O_2	150	32.77	67.23	0.49
	250	32.84	67.16	0.49
	350	32.98	67.02	0.49

DOI: 10.1021/acs.chemmater.8b05282
Chem. Mater. 2019, 31, 3900−3908

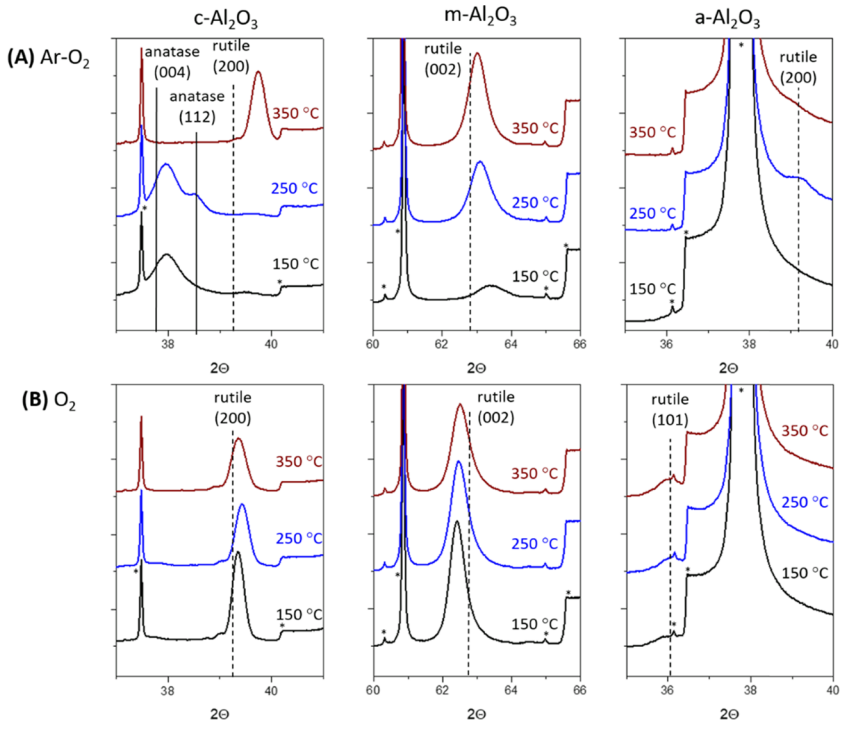

Figure 2. XRD of TiO_2 grown by ALD on *c*-, *m*-, and *a*-Al_2O_3 using (A) Ar−O_2 and (B) O_2 plasma at 150, 250, and 350 °C. Solid and dashed lines correspond to the relaxed peak position for the labeled anatase and rutile TiO_2, respectively. Features due to the sapphire substrate are labeled with *.

deposited films likely results from the atmospheric transfer of the sample from the ALD chamber to the XPS chamber. However, there is no indication of the residual carbon from the metal organic precursors in the bulk of the films deposited. The concentrations of Ti and O, from Ti 2p and O 1s scans, respectively, are shown in Table 1 and demonstrate a nearly stoichiometric Ti/O ratio of 0.49 for all TiO_2 films.

By depositing on *c*-, *m*-, and *a*-Al_2O_3 substrates simultaneously, the effect of the underlying substrate can be accurately evaluated along with the effect of growth temperature and gas chemistry. To better demonstrate and compare the effect of these growth variables (i.e., temperature, gas chemistry, and substrate orientation), all XRD will be plotted together, see Figure 2. The films grown using traditional Ar−O_2 plasma chemistry to address the effect of temperature will be evaluated first (Figure 2A), whereas the effect of O_2 plasma chemistry (Figure 2B) will be addressed later.

EFFECT OF TEMPERATURE

Previously published work demonstrated that epitaxial TiO_2 on *c*-Al_2O_3 could be attained using PE-ALD and TDMAT at temperatures as low as 250 °C, and the phase grown was dependent on the reaction temperature.[16,18] Similar parameters were explored here as a function of the sapphire substrate orientation. As the XRD data in Figure 2 illustrates, the underlying substrate can cause significant variations in the film quality. All films deposited were highly oriented with only one out-of-plane peak corresponding to the TiO_2 film present. For the rutile films on *c*-Al_2O_3, the second-order peak, (400) 84.43° indicating the high crystalline quality of these thin films. Since 2θ measurements were only taken to 90°, no second-order peaks were detected for TiO_2 on *m*-plane, and the poor crystallinity of films on *a*-Al_2O_3 prevented higher order peaks from being identified. Table 2 summarizes the peak location, film orientation, and strain for all data shown in Figure 2.

Table 2. XRD Peak Values and Calculated Strain from Figure 2

substrate	plasma gas	phase (peak)	T_g (°C)	20 (deg)	FWHM (deg)	ε (%)
c-Al_2O_3	Ar−O_2	anatase (004)	150	37.97	0.48	−0.43
		anatase (004)	250	37.96	0.39	−0.41
		anatase (112)	250	38.84	0.33	−0.67
		rutile (200)	350	39.74	0.3	−1.31
	O_2	rutile (200)	150	39.36	0.26	−0.39
		rutile (200)	250	39.43	0.29	−0.56
		rutile (200)	350	39.37	0.32	−0.41
m-Al_2O_3	Ar−O_2	rutile (002)	150	63.44	0.95	−0.93
		rutile (002)	250	63.12	0.7	−0.48
		rutile (002)	350	63.02	0.62	−0.34
	O_2	rutile (002)	150	62.44	0.55	0.49
		rutile (002)	250	62.49	0.61	0.42
		rutile (002)	350	62.53	0.63	0.36
a-Al_2O_3	Ar−O_2	NA	150			
		rutile (200)	250	39.68	0.48	−1.16
		rutile (200)	350	38.54	2.13	1.65
	O_2	rutile (101)	150	36.14	0.97	−0.13
		rutile (101)	250	36.12	0.68	−0.08
		rutile (101)	350	36.07	0.7	0.05

Figure 2A shows the structure of TiO_2 films grown using a typical Ar−O_2 mixed plasma for various sapphire substrate orientations. Although crystalline films were achieved at all temperatures on *c*-Al_2O_3 substrates, there was a large phase dependence on temperature. In comparison, there is no phase change observed on the other planes of the sapphire regardless of the growth temperature indicating that the behavior observed on *c*-Al_2O_3 substrates is unique to that plane. At 150 °C, the films

DOI: 10.1021/acs.chemmater.8b05282
Chem. Mater. 2019, 31, 3900−3908

are anatase, as indicated by the (004) peak at 37.97°. Comparing this peak location to the relaxed anatase (004) at 37.80°,[23] results in a compressive strain of −0.43% (Table 2). Increasing the temperature to 250 °C results in a polycrystalline anatase phase with orientations (004) at 37.97° and (112) at 38.84°. However, by 350 °C, only a sharp rutile (200) peak observed at 39.74°. The rutile (200) peak is noticeably shifted to higher 2θ equating to a compressive strain of −1.3%.[24] It should be noted that the anatase phase exhibits broader peaks than the higher temperature rutile phase, with full width half maximum (FWHM) of 0.48 and 0.39° for anatase (004) at 150 and 250 °C, respectively, and a FWHM of 0.3° for rutile (200) at 350 °C. This suggests a higher crystalline quality for the rutile TiO_2 films, though it is difficult to determine if this is an effect of the higher growth temperature or the phase itself. More importantly, these results show that for TiO_2 grown on c-Al_2O_3 using an Ar−O_2 plasma, the phase can be tuned between high-quality single-phase anatase and rutile simply with growth temperature.

Unlike TiO_2 films on c-Al_2O_3, films deposited on m-Al_2O_3 result in the rutile phase with Ar−O_2 plasma at all temperatures. The lack of phase selectivity in this orientation can be attributed to closer lattice matching of the rutile TiO_2 to m-Al_2O_3, −3.5%, which is significantly less than the 6% mismatch to c-Al_2O_3.[25] However, the film crystallinity and strain are temperature dependent. At 150 °C, a low-intensity, broad peak at 63.44° is indicative of a rutile (002) phase with little crystallinity and compressively strained −0.93%. By increasing the temperature to 250 °C, the rutile (002) peak increases in intensity and shifts to 63.12°, representing a decrease in the compressive strain to −0.48%. This more intense peak had a FWHM of 0.7°, which is smaller than the FWHM of 0.95° for TiO_2 grown at 150 °C. Further increasing the growth temperature to 350 °C yields a sharper, more intense, rutile (002) peak, with a FWHM of 0.62°, located at 63.02°, indicating the lowest compressive strain of −0.34% for TiO_2 on m-Al_2O_3. The increase in the peak intensity, the decrease in FWHM, and the reduction in the compressive strain suggest that better TiO_2 film quality is achieved when films are grown at higher temperatures using Ar−O_2 plasma on the m-plane sapphire. Nevertheless, to deposit the anatase phase, TiO_2 films would require excluding m-Al_2O_3 as a possible substrate.

TiO_2 grown on a-Al_2O_3 shows a different scenario to films grown on c- and m-Al_2O_3, with all films resulting in a low degree of crystallinity (Figure 2A). At 150 °C, there is no noticeable peak present, but TiO_2 films grown at 250 °C yield a peak at 39.68° indicating a small fraction of rutile (200) phase with a compressive strain of −1.16%. Increasing the growth temperature further to 350 °C results in a reduction in the intensity of the rutile (200) peak and a shift to 38.54°, signifying a tensile strain of 1.65%. The low-intensity peaks in the XRD would indicate a film of low crystallinity, and the broadness of the peaks suggests that the crystallinity is highly defective (i.e., nonuniform strain). The proximity of the underlying sapphire peaks makes it difficult to resolve the low-intensity rutile (200) peaks, but HRXRD (Figure 3A) was used to confirm the presence of the rutile (200) peak for films grown at 350 °C. These results show that the influence of the substrate on the ability to achieve crystalline films at low temperatures with the phase selectivity is highly dependent on the underlying substrate.

Raman spectroscopy was also used to evaluate the crystalline phase of the TiO_2 deposited in this study. Figure 4A shows the Raman spectra of TiO_2 grown on c-, m-, and a-Al_2O_3 using Ar−O_2 plasma as a function of the deposition temperature. As with

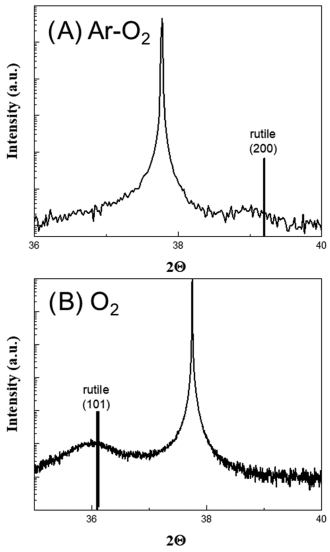

Figure 3. HRXRD of TiO_2 grown at 350 °C on a-Al_2O_3 using (A) Ar−O_2 and (B) O_2 plasma.

the XRD spectra in Figure 2, the Raman spectra of films deposited with O_2 plasma, Figure 4B, will be addressed later. In general, the change observed in the Raman peak position and intensity correlates well with the trends in XRD. Films deposited at 150 and 250 °C on c-Al_2O_3 showed a pure anatase phase with peaks at 637, 519, 399, and 143 cm^{-1}, corresponding to bonding modes E_g, $A_{1g} + B_{1g}$, B_{1g}, and E_g.[26] The peak intensities increase with the increasing temperature from 150 to 250 °C, similar to the XRD peaks above. At 350 °C, films exhibited a pure rutile phase with peaks at 595, 425, and 149 cm^{-1}, which correspond to bonding modes A_{1g}, E_g, and B_{1g}.[26] A peak at 320 cm^{-1} was also detected, and although the peak is associated with TiO_2 films, it does not correspond to a known bonding mode. However, these Raman results confirm the XRD results that crystalline films are achieved at all temperatures, and the phase selectivity can be controlled with the growth temperature.

For TiO_2 films on m-Al_2O_3, Raman spectra show only the rutile phase at all temperatures, with peaks at 614 and 448 cm^{-1}, corresponding to the A_{1g} and E_g bonding modes.[26] The 614 cm^{-1} peak increased in the intensity with the increasing growth temperature similar to the XRD results (Figure 2A). The Raman spectrum of TiO_2 grown on m-Al_2O_3 at 250 °C also has a small rutile peak at 144 cm^{-1}, corresponding to a B_{1g} and observed for rutile TiO_2 films grown on c-Al_2O_3, but this peak was not observed in any other rutile spectrum of TiO_2 on m- or a-Al_2O_3 substrates. Additionally, the peak at 448 cm^{-1} (matched to the symmetric E_g bonding mode) decreases in the intensity with the increasing deposition temperature until it is no longer present in at 350 °C. Films deposited at 350 °C showed the highest degree of crystallinity, suggesting that the 448 cm^{-1} peak is a structural defect, rather than an E_g bonding mode, which is no longer present in films deposited at higher temperatures.

Similar to the Raman spectra of TiO_2 on m-Al_2O_3, TiO_2 grown using Ar−O_2 plasma on a-Al_2O_3 indicated that the rutile phase was present at all temperatures, with small peaks at 612 and 448 cm^{-1}, corresponding to the A_{1g} and E_g bonding modes. Despite the low-intensity XRD peaks (Figure 2A), the Raman spectrum in Figure 3A confirms that the films grow purely rutile TiO_2 on a-Al_2O_3 for all conditions. Also, the most clearly defined Raman intensities of the TiO_2 films grown on a-Al_2O_3 were grown at 250 °C, which correlates well with XRD. Although

DOI: 10.1021/acs.chemmater.8b05282
Chem. Mater. 2019, 31, 3900−3908

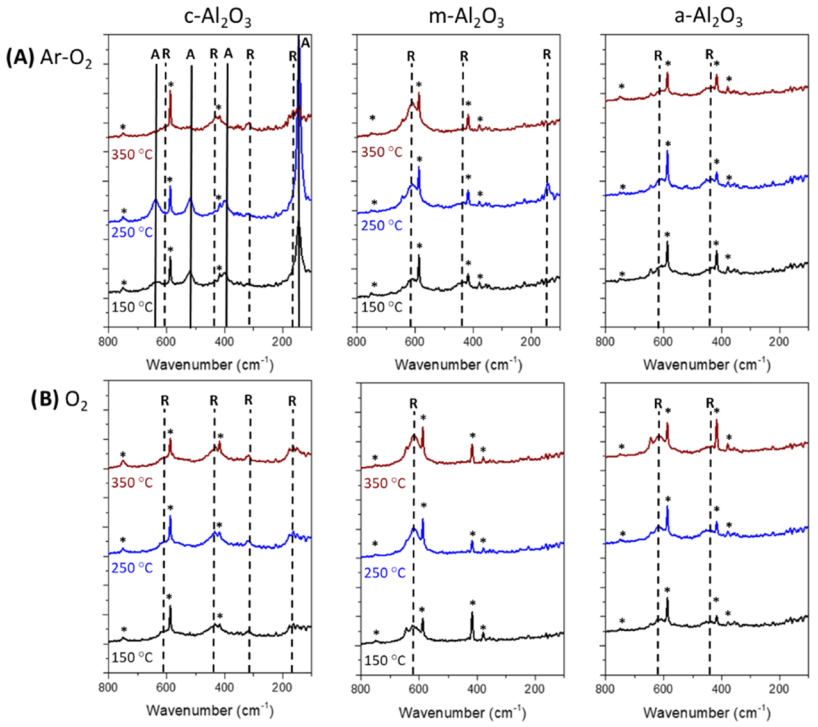

Figure 4. Raman spectrum of TiO_2 grown on *c*-, *m*-, and *a*-plane Al_2O_3 using (A) Ar−O_2 and (B) O_2 plasma at 150−350 °C. (*) indicated peaks from the underlying sapphire and the solid and dashed lines indicate anatase and rutile peaks, respectively.

XRD would indicate no long-range order in the TiO_2 films grown on *a*-Al_2O_3, this does not rule out nanocrystallinity in the deposited films.

AFM images in Figure 5 demonstrate the impact of that substrate and growth temperature, using Ar−O_2 plasma, on the TiO_2 film morphology. For TiO_2 grown on *c*-Al_2O_3, the roughness decreases with the increasing temperature from 1.44 nm at 150 °C to 1.38 nm at 250 °C and 1.05 nm at 350 °C. The reduction in roughness between 150 and 250 °C for TiO_2 films grown on *c*-Al_2O_3 is modest; however, there is a larger reduction in the roughness at 350 °C, the temperature at which films deposit rutile. Given that the TiO_2 deposited on *c*-Al_2O_3 changed from anatase to mixed orientation to rutile from 150 to 350 °C, the decreasing roughness from Figure 5 suggests that rutile TiO_2 films are less rough. TiO_2 on *m*-Al_2O_3, which were all determined to be rutile, further demonstrates this with a lower roughness of 0.54 nm for the film deposited at 150 °C. However, there was a significant increase in the film roughness to 1.60 nm for films grown at 250 °C (Figure 5), followed by a decrease in the roughness to 0.67 nm when the TiO_2 films are grown at 350 °C. TiO_2 on *a*-Al_2O_3 substrates show a similar behavior to films grown on *m*-Al_2O_3. TiO_2 film on *a*-Al_2O_3 at 150 °C had a roughness of 0.58 nm, which is similar roughness to TiO_2 grown on *m*-Al_2O_3 and lower than TiO_2 grown on *c*-Al_2O_3. Increasing the growth temperature to 250 °C increases the roughness to 0.85 nm, but the roughness was then reduced to 0.60 nm when grown at 350 °C. With the exception of the TiO_2 film on *m*-Al_2O_3 at 250 °C, the lower roughnesses of films deposited on *m*- and *a*-Al_2O_3 compared to TiO_2 on *c*-Al_2O_3 at 150 and 250 °C suggest that in general rutile films result in smoother morphologies than anatase films.

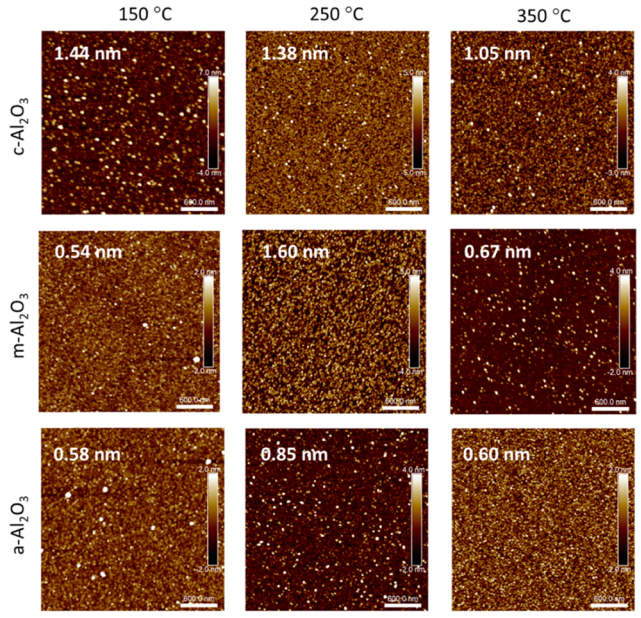

Figure 5. AFM of TiO_2 grown on *c*-, *m*-, and *a*-plane Al_2O_3 using Ar−O_2 mixed plasma at 150−350 °C. The root mean square (RMS) roughness of image displayed in the top left-hand corner of each image. All scale bars (lower right of each image) are 600 nm. Scan size was 3 × 3 μm^2.

From the above results, it is clear that the growth temperature plays an important role in the film quality and phase. For *c*-Al_2O_3, TiO_2 grows in different phases depending on the growth temperature, whereas films grown on *m*- and *a*-Al_2O_3 only grow rutile, but the quality and strain vary with growth temperature, demonstrating that the underlying substrate also plays an important role.

DOI: 10.1021/acs.chemmater.8b05282
Chem. Mater. 2019, 31, 3900−3908

EFFECT OF GAS CHEMISTRY

Increasing the concentration of atomic oxygen in the plasma chemistry also has a significant impact, thus examining the effect of gas chemistry on TiO_2 phase, and the crystallinity was investigated as a function of the substrate orientation and deposition temperature, (Figures 2B and 4B). As evidenced in the XRD spectra in Figure 2, TiO_2 films grown on c-Al_2O_3 with an Ar−O_2 plasma (Figure 2A) or an O_2 plasma (Figure 2B) result in vastly different evolutions of the phase with temperature. Films produced using a pure O_2 plasma yielded rutile (200) for all growth temperatures and, in general, exhibited a less compressive strain (Table 2). For example, the direct comparison of rutile films grown at 350 °C with the two gas chemistries have compressive strains of −0.41 and −1.3% for O_2 and Ar−O_2 plasmas, respectively. Specifically for films grown with O_2 plasma on c-Al_2O_3, the compressive strain was small, ranging from −0.39 to −0.56% with a minimal deviation with the changing deposition temperature. However, the rutile (200) peak does have a substantial variation in the intensity and FWHM with the growth temperature. The crystalline quality of the films decreases with the increasing growth temperature, inferred by the reduction in the XRD peak intensity and the FWHM to increase from 0.26 to 0.32°. This indicates that higher quality rutile films are achieved at lower temperatures than previously published methods using Ar−O_2 plasma chemistry where crystalline films were only attained at 250−300 °C.[18,20,22]

TiO_2 films deposited on m-Al_2O_3 substrates using a pure O_2 plasma have a rutile (002) orientation for all growth temperatures, similar to that achieved with the Ar−O_2 plasma. The primary difference between films grown with different gas chemistries is the strain state, which switches from compressive with Ar−O_2 plasma to tensile strain with pure O_2 plasma. For example, films deposited at 350 °C changed from a compressive strain of −0.34% to a tensile strain of 0.49% for an Ar−O_2 or O_2 plasma, respectively. Furthermore, increasing the growth temperature leads to a slight reduction in the tensile strain, decreasing from 0.49 to 0.36% from 150 to 350 °C. These results demonstrate that gas chemistry has a greater effect than the growth temperature on TiO_2 strain for films grown on m-Al_2O_3. Similar to the rutile films grown on c-Al_2O_3 using O_2 plasma, increasing the deposition temperature also causes a decrease in the peak intensity and the FWHM to increase from 0.55 to 0.63° from 150 to 350 °C, suggesting that higher quality films are attained at lower temperatures.

Films grown on a-Al_2O_3 show a different rutile orientation depending on the plasma chemistry used (Figure 2). For TiO_2 grown using Ar−O_2 plasma (Figure 2A), a weak rutile (200) peak is observed only at higher temperatures (250−350 °C). However, for films deposited with a pure O_2 plasma, a rutile (101) peak is observed at 36.0° for all growth temperatures implemented in this study, and the peak intensity increases with increasing growth temperatures. A direct comparison of the HRXRD in Figure 3 clearly indicates a change in the TiO_2 orientation with a low-intensity rutile (200) peak at 39.0° for films grown using Ar−O_2 plasma and a rutile (101) peak at 36.2° for films grown using O_2 plasma. The broad shape and low intensity of the peaks in both low-resolution XRD and HRXRD (see Figure 3) indicate that TiO_2 films grown on a-Al_2O_3 are of lower crystalline quality, than films grown simultaneously on m- and c-Al_2O_3. The broadness of the peaks makes it difficult to determine the film strain, but a-Al_2O_3 is the only substrate for which TiO_2 changes orientation between Ar−O_2 and O_2 plasma gas chemistry.

Raman spectroscopy of TiO_2 films grown using O_2 plasma confirms that only rutile phase films are grown independent of the temperature or substrate orientation, Figure 4B. Raman spectra of TiO_2 grown on c-Al_2O_3 using pure O_2 shows the same rutile peaks (149, 320, 425, and 595 cm^{-1}) observed for films grown at 350 °C using Ar−O_2 plasma (Figure 4A). It should be noted, similar to the XRD spectrum in Figure 2B, the Raman spectrum for TiO_2 on c-Al_2O_3 did not change with the increasing temperature when grown with O_2 plasma. On m-Al_2O_3 substrates, the Raman spectra of TiO_2 films grown using O_2 plasma showed only the A_{1g} peak at 614 cm^{-1} and does not exhibit the E_g peak at 448 cm^{-1}, which is similar to the TiO_2 films grown using Ar−O_2 on m-Al_2O_3 at 350 °C, suggesting that all TiO_2 films grown on m-Al_2O_3 are less defective when using O_2 plasma. The TiO_2 films grown on a-Al_2O_3 using O_2 plasma have similar Raman spectra to their Ar−O_2 counterparts, with peaks at 612 and 448 cm^{-1}. However, for the films grown with O_2 plasma, the A_{1g} peak at 614 cm^{-1} increases in the intensity with higher growth temperature correlating with an increasing rutile (101) peak intensity seen in Figure 2B. In addition, Raman spectra of TiO_2 on a-Al_2O_3 confirms crystallinity at even the lowest growth temperature (150 °C), though only a minimal peak is exhibited in the XRD spectra.

The XRD and Raman spectra shown in Figures 2 and 4 are strong evidence that the TiO_2 grown using PE-ALD can grow crystalline, as deposited. To assess the epitaxial nature of the films grown asymmetric, HRXRD scans were taken on the high-quality TiO_2 films on the c- and m-plane sapphire deposited at 150 °C using O_2. From Figure 6A,B asymmetric scans, we can

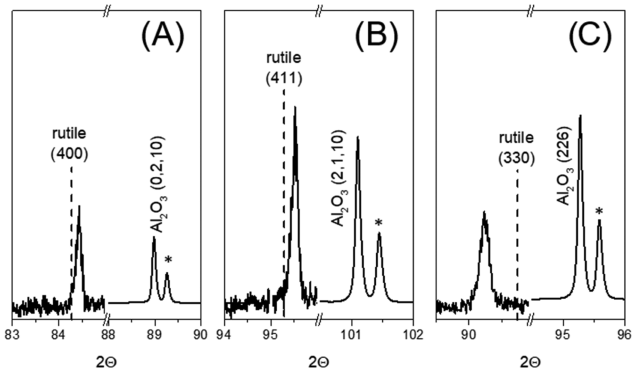

Figure 6. Asymmetric HRXRD spectra of PE-ALD TiO_2 films grown using O_2 plasma at 150 °C on (A + B) c-Al_2O_3 and (C) m-Al_2O_3. (*) kβ peak from the X-ray source.

see that TiO_2 films on c-Al_2O_3 have the following alignments: (0,2,10)//(400) and (2,1,10)//(411). These alignments correspond to the out-of-plane alignment (006)//(200) observed in the XRD spectra in Figure 2B. Figure 6C shows that the TiO_2 film deposited on m-Al_2O_3 yielded an alignment of (226)//(330), which correspond to the out-of-plane alignment (300)//(002) (Figure 2B). As Figure 6 illustrates, the asymmetric measurements result in only a single TiO_2 peak for each condition corresponding to the rutile phase. Additionally, the rutile peaks shown only appear when the sample is tilted to the specific corresponding sapphire peak. GID measurements (not shown) conducted on TiO_2 film on c-Al_2O_3 in Figure 6A,B produced only slightly elongated spots with no trace of diffraction rings, characteristic of textured or polycrystalline

DOI: 10.1021/acs.chemmater.8b05282
Chem. Mater. 2019, 31, 3900−3908

films. Thus, from these asymmetric and GID results, the as-deposited TiO_2 films are epitaxial and not textured. This shows that the deposition technique demonstrated here using a pure O_2 plasma is capable of growing epitaxial rutile TiO_2 films as low as 150 °C.

A pure O_2 plasma also affects the TiO_2 film morphology. Figure 7 shows AFM images of TiO_2 grown with O_2 plasma for

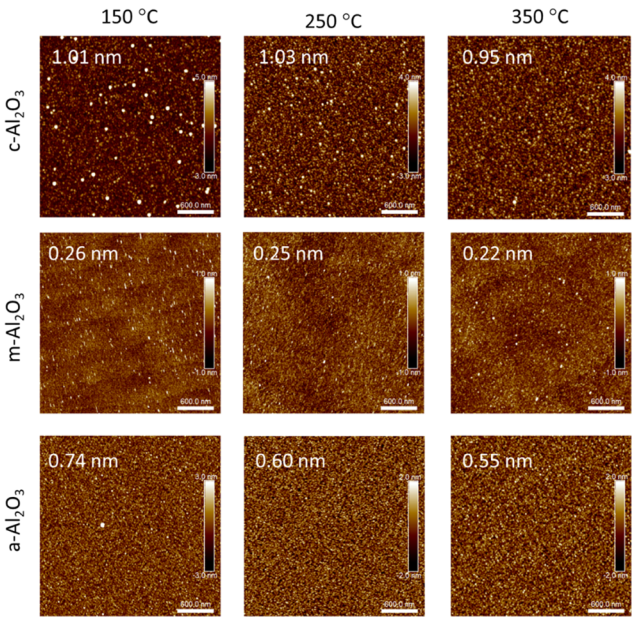

Figure 7. AFM of TiO_2 grown on *c*-, *m*-, and *a*-plane Al_2O_3 using O_2 plasma at 150, 250, and 350 °C. The RMS roughness of the image displayed in the top left-hand corner of each image. All scale bars (lower right of each image) are 600 nm. Scan size was 3 × 3 μm^2.

all substrate orientations and deposition temperatures. Unlike with an Ar−O_2 plasma, there is a very little change due to the deposition temperature on the TiO_2 film morphology when using O_2 plasma. For instance, on *c*-Al_2O_3, films demonstrated a roughness reduction of only 0.06 nm from 1.01 to 0.95 nm as the growth temperature was increased from 150 to 350 °C. Similarly, there was a negligible difference in the film roughness for TiO_2 grown on *m*-Al_2O_3, indicating that the growth temperature has a minimal effect on the film morphology when O_2 plasma is used. On *a*-Al_2O_3, there was a slight reduction in the film roughness with the increasing growth temperature when using O_2 plasma, but the overall roughness was similar to films grown using Ar−O_2 plasma. Addressing the effect of gas chemistry, films deposited on *c*- and *m*-Al_2O_3 with an O_2 plasma are smoother than films produced with the Ar−O_2 plasma, whereas the roughness of TiO_2 films on *a*-Al_2O_3 is independent of plasma gas chemistry. An example of this can be seen for films grown at 150 °C, with O_2 plasma showing a roughness of 0.26 nm, which is nearly half of the 0.54 nm for films grown using Ar−O_2 on *m*-Al_2O_3. As seen in Figure 7, the underlying step morphology is clearly visible for TiO_2 grown on *m*-Al_2O_3 at 150 °C. Given the minimal effect of the growth temperature when using the O_2 plasma, the underlying substrate has a greater effect on the film roughness, with *m*-Al_2O_3 yielding the smoothest film and *c*-Al_2O_3 yielding the roughest.

The above results show that using a pure O_2 plasma instead of ArO_2 plasma gas chemistry is beneficial to facilitate high-quality, epitaxial rutile TiO_2 films at low temperatures with a lower film roughness. Assessing the effect of the plasma composition on the films grown is an ongoing study, but the preliminary optical emission spectroscopy analysis (not shown) of the plasma source indicates that the ratio of excited atomic oxygen over excited molecular oxygen is 3 times for the pure O_2 plasma case relative to the Ar−O_2 plasma case. Additionally, preliminary Langmuir probe measurements indicate that the O_2 plasma has a significantly higher plasma potential compared to the Ar−O_2 plasma. At these relatively low operating pressures, this likely leads to a higher ion energy at the growth surface. The combination of these effects resulted in higher quality films being deposited using pure O_2 plasma over films grown using the Ar−O_2 plasma, especially at very low temperatures. However, when using the O_2 plasma, there is no control over the phase and little control over the strain under these conditions, with strain relying more on the substrate than the temperature when using O_2 plasma.

EFFECT OF PHASE ON OPTICAL PROPERTIES

CL was implemented to analyze the defects present in the TiO_2 films grown on *c*-Al_2O_3 by measuring deep level states. Cryogenic (5 K) CL spectra shown in Figure 8 indicate no

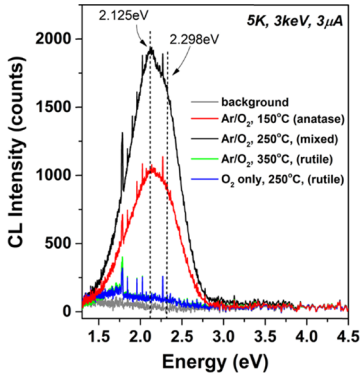

Figure 8. Cathodoluminescence of TiO_2 grown on *c*-Al_2O_3 at 150, 250, and 350 °C using Ar−O_2 plasma and O_2 plasma. The phase is listed in the parenthesis for each condition. CL measured at 5 K, with an operating (accelerating) voltage of 3 keV and 3 μA beam current.

band-to-band transitions for any of the spectra measured. As Figure 8 demonstrates, anatase and mixed orientation films grown at 150 and 250 °C with Ar−O_2 plasma exhibited the largest sub-bandgap luminescence. In contrast, rutile TiO_2, grown at 350 and 250 °C using Ar−O_2 and O_2 plasma, respectively, showed a negligible luminescence. The similarities in luminescence for both rutile films in Figure 8 demonstrate that the gas chemistry used during the ALD process does not affect the optical properties of the rutile films grown. The presence of a higher luminescence peak for anatase films indicates a higher density of structural defects in the TiO_2 film.[28,29] Previous reports have indicated that an incomplete or strained coordination between Ti and O atoms in the structure will cause sub-bandgap states to form in the bandgap of the TiO_2.[15,27] Hence, CL demonstrates that anatase films contain more point defects than the rutile films grown in this study.[28,29]

CONCLUSIONS

PE-ALD was utilized to achieve high-quality epitaxial TiO_2 films at temperatures as low as 150 °C. Substrate, growth temperature, and gas chemistry had varying levels of impact on phase

DOI: 10.1021/acs.chemmater.8b05282
Chem. Mater. 2019, 31, 3900−3908

selectivity of TiO_2. TiO_2 grown using a typical $Ar-O_2$ plasma yield very different phases and structures depending on the sapphire substrate orientation it was deposited on and the growth temperature. On *c*-Al_2O_3, TiO_2 phase selectivity is attained by varying the deposition temperature, resulting in single-phase anatase films at 150 °C and rutile films at 350 °C. The same plasma conditions on *m*- and *a*-Al_2O_3 produced only rutile TiO_2 independent of the growth temperature, but increasing the deposition temperature improved the crystalline quality and reduces strain. Using $Ar-O_2$ plasma, *c*-Al_2O_3 was the only substrate to observe the phase selectivity, demonstrating the importance of the underlying substrate on the deposited TiO_2 film. Employing a pure O_2 plasma resulted in rutile phase films for all substrates and growth temperatures explored, showing the inability to attain phase selectivity with this plasma gas chemistry. However, a pure O_2 plasma was important in achieving higher crystalline quality at low growth temperatures, with the confirmed epitaxial alignment of (0,2,10)//(400) and (2,1,10)//(411) on *c*-Al_2O_3 and (226)//(330) on *m*-Al_2O_3. Additionally, varying the gas chemistry and substrate orientation allows the adjustment of the film strain from tensile to compressive, enabling the ability to tailor strain in TiO_2 films for different applications. Finally, TiO_2 films on *a*-Al_2O_3 exhibited significantly less crystallinity than other sapphire orientations independent of the growth temperature and gas chemistry, emphasizing the importance of consideration in the underlying substrate to promote the desired material quality. These results demonstrate the benefits of the PE-ALD method to control TiO_2 film crystallinity, phase, strain, and morphology through tuning of basic growth conditions.

AUTHOR INFORMATION

Corresponding Author

*E-mail: virginia.wheeler@nrl.navy.mil. Phone: (202) 404-4450.

ORCID

Jason R. Avila: 0000-0002-0478-5875

Virginia D. Wheeler: 0000-0002-6024-9516

Author Contributions

All authors have given approval to the final version of the manuscript.

Notes

The authors declare no competing financial interest.

ACKNOWLEDGMENTS

Funding for this research was provided by the Office of Naval Research. J.R.A. acknowledges support from the American Society for Engineering Education Postdoctoral Fellowship.

REFERENCES

(1) Glassford, K. M.; Chelikowsky, J. R. Structural and electronic properties of titanium dioxide. *Phys. Rev. B* **1992**, *46*, 1284−1298.

(2) Schneider, J.; Matsuoka, M.; Takeuchi, M.; Zhang, J.; Horiuchi, Y.; Anpo, M.; Bahnemann, D. W. Understanding TiO2 Photocatalysis: Mechanisms and Materials. *Chem. Rev.* **2014**, *114*, 9919−9986.

(3) Bae, G.; Song, Y.; Jung, D.; Roh, Y. Significant reduction of leakage current in the TiO2/Si structure by the insertion of the CeO2 intermediate layer. *Appl. Phys. Lett.* **2000**, *77*, 729−731.

(4) Luan, H. F.; Mao, A. Y.; Lee, S. J.; Luo, T. Y.; Kwong, D. L. Ultrathin TiO2 Gate Dielectric Formation by Annealing of Sputtered Ti on Nitrogen Passivated Si Substrates in Nitric Oxide Ambient. *MRS Online Proc. Libr. Arch.* **2011**, *567*, No. 481.

(5) Lee, M. M.; Teuscher, J.; Miyasaka, T.; Murakami, T. N.; Snaith, H. J. Efficient Hybrid Solar Cells Based on Meso-Superstructured Organometal Halide Perovskites. *Science* **2012**, *338*, 643−647.

(6) Bai, Y.; Mora-Seró, I.; De Angelis, F.; Bisquert, J.; Wang, P. Titanium Dioxide Nanomaterials for Photovoltaic Applications. *Chem. Rev.* **2014**, *114*, 10095−10130.

(7) Yang, W.; Monson, A.; Marino, J.; Wolden, C. A. Optimizing the dielectric performance of TiO2 thin films through control of plasma-enhanced chemical vapor deposition process conditions. *J. Vac. Sci. Technol., A* **2007**, *25*, 1298−1301.

(8) Abendroth, B.; Moebus, T.; Rentrop, S.; Strohmeyer, R.; Vinnichenko, M.; Weling, T.; Stöcker, H.; Meyer, D. C. Atomic layer deposition of TiO2 from tetrakis(dimethylamino)titanium and H2O. *Thin Solid Films* **2013**, *545*, 176−182.

(9) Möldre, K.; Aarik, L.; Mändar, H.; Niilisk, A.; Rammula, R.; Tarre, A.; Aarik, J. Atomic layer deposition of rutile and TiO2-II from TiCl4 and O3 on sapphire: Influence of substrate orientation on thin film structure. *J. Cryst. Growth* **2015**, *428*, 86−92.

(10) Kukli, K.; Aidla, A.; Aarik, J.; Schuisky, M.; Hårsta, A.; Ritala, M.; Leskelä, M. Real-Time Monitoring in Atomic Layer Deposition of TiO2 from TiI4 and H2O−H2O2. *Langmuir* **2000**, *16*, 8122−8128.

(11) Schuisky, M.; Aarik, J.; Kukli, K.; Aidla, A.; Hårsta, A. Atomic Layer Deposition of Thin Films Using O2 as Oxygen Source. *Langmuir* **2001**, *17*, 5508−5512.

(12) Tarre, A.; Möldre, K.; Niilisk, A.; Mändar, H.; Aarik, J.; Rosental, A. Atomic layer deposition of epitaxial TiO2 II on c-sapphire. *J. Vac. Sci. Technol., A* **2013**, *31*, No. 01A118.

(13) Schuisky, M.; Kukli, K.; Aarik, J.; Lu, J.; Hårsta, A. Epitaxial growth of TiO2 films in a hydroxyl-free atomic layer deposition process. *J. Cryst. Growth* **2002**, *235*, 293−299.

(14) Ritala, M.; Leskela, M.; Niinisto, L.; Haussalo, P. Titanium isopropoxide as a precursor in atomic layer epitaxy of titanium dioxide thin films. *Chem. Mater.* **1993**, *5*, 1174−1181.

(15) Das, C.; Henkel, K.; Tallarida, M.; Schmeißer, D.; Gargouri, H.; Kärkkänen, I.; Schneidewind, J.; Gruska, B.; Arens, M. Thermal and plasma enhanced atomic layer deposition of TiO2: Comparison of spectroscopic and electric properties. *J. Vac. Sci. Technol., A* **2015**, *33*, No. 01A144.

(16) Schindler, P.; Logar, M.; Provine, J.; Prinz, F. B. Enhanced Step Coverage of TiO2 Deposited on High Aspect Ratio Surfaces by Plasma-Enhanced Atomic Layer Deposition. *Langmuir* **2015**, *31*, 5057−5062.

(17) Choi, G.-J.; Kim, S. K.; Won, S.-J.; Kim, H. J.; Hwang, C. S. Plasma-Enhanced Atomic Layer Deposition of TiO2 and Al-Doped TiO2 Films Using N2O and O2 Reactants. *J. Electrochem. Soc.* **2009**, *156*, G138−G143.

(18) Pointet, J.; Gonon, P.; Latu-Romain, L.; Bsiesy, A.; Vallée, C. Rutile-structured TiO2 deposited by plasma enhanced atomic layer deposition using tetrakis(dimethylamino)titanium precursor on in-situ oxidized Ru electrode. *J. Vac. Sci. Technol., A* **2014**, *32*, No. 01A120.

(19) Chaker, A.; Szkutnik, P. D.; Pointet, J.; Gonon, P.; Vallée, C.; Bsiesy, A. Understanding the mechanisms of interfacial reactions during TiO2 layer growth on RuO2 by atomic layer deposition with O2 plasma or H2O as oxygen source. *J. Appl. Phys.* **2016**, *120*, No. 085315.

(20) Kassmi, M.; Pointet, J.; Gonon, P.; Bsiesy, A.; Vallée, C.; Jomni, F. Low-frequency dielectric properties of intrinsic and Al-doped rutile TiO2 thin films grown by the atomic layer deposition technique. *J. Appl. Phys.* **2016**, *119*, No. 244101.

(21) Profijt, H. B.; van de Sanden, M. C. M.; Kessels, W. M. M. Substrate Biasing during Plasma-Assisted ALD for Crystalline Phase-Control of TiO2 Thin Films. *Electrochem. Solid-State Lett.* **2011**, *15*, G1−G3.

(22) Faraz, T.; Knoops, H. C. M.; Verheijen, M. A.; van Helvoirt, C. A. A.; Karwal, S.; Sharma, A.; Beladiya, V.; Szeghalmi, A.; Hausmann, D. M.; Henri, J.; Creatore, M.; Kessels, W. M. M. Tuning Material Properties of Oxides and Nitrides by Substrate Biasing during Plasma-Enhanced Atomic Layer Deposition on Planar and 3D Substrate Topographies. *ACS Appl. Mater. Interfaces* **2018**, *10*, 13158−13180.

(23) *ICSD*, PDF 01-078-1508; Fiz Karlsruhe: Eggenstein-Leopoldshafen: Germany, 1998 (July 4, 2017).

DOI: 10.1021/acs.chemmater.8b05282
Chem. Mater. 2019, 31, 3900−3908

(24) *ICSD*, PDF 01-078-1508; Fiz Karlsruhe: Eggenstein-Leopoldshafen: Germany, 1998 (July 4, 2017).
(25) Silva, V. F.; Bouquet, V.; Deputier, S.; Boursicot, S.; Ollivier, S.; Weber, I. T.; Silva, V. L.; Santos, I. M. G.; Guilloux-Viry, M.; Perrin, A. Substrate-controlled allotropic phases and growth orientation of TiO2 epitaxial thin films. *J. Appl. Crystallogr.* **2010**, *43*, 1502−1512.
(26) Frank, O.; Zukalova, M.; Laskova, B.; Kürti, J.; Koltai, J.; Kavan, L. Raman spectra of titanium dioxide (anatase, rutile) with identified oxygen isotopes (16, 17, 18). *Phys. Chem. Chem. Phys.* **2012**, *14*, 14567−14572.
(27) Avila, J. R.; Katz, M. J.; Farha, O. K.; Hupp, J. T. Barrier-Layer-Mediated Electron Transfer from Semiconductor Electrodes to Molecules in Solution: Sensitivity of Mechanism to Barrier-Layer Thickness. *J. Phys. Chem. C* **2016**, *120*, 20922−20928.
(28) Suisalu, A.; Aarik, J.; Mändar, H.; Sildos, I. Spectroscopic study of nanocrystalline TiO2 thin films grown by atomic layer deposition. *Thin Solid Films* **1998**, *336*, 295−298.
(29) Stevanovic, A.; Büttner, M.; Zhang, Z.; Yates, J. T. Photoluminescence of TiO2: Effect of UV Light and Adsorbed Molecules on Surface Band Structure. *J. Am. Chem. Soc.* **2012**, *134*, 324−332.

DOI: 10.1021/acs.chemmater.8b05282
Chem. Mater. 2019, 31, 3900−3908